Applied Surface Science 654 (2024) 159442

Contents lists available at ScienceDirect

Applied Surface Science

journal homepage: www.elsevier.com/locate/apsusc

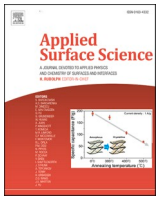

Full Length Article

Electrochemically generated CuI and CuSCN nanocrystals on Cu surfaces as Raman enhancing substrates

Martin Perez-Estebanez [a,*], William Cheuquepan [a,b,c,1], Aranzazu Heras [a], Alvaro Colina [a,*]

[a] Department of Chemistry, Universidad de Burgos, Pza. Misael Bañuelos s/n, E-09001 Burgos, Spain
[b] Bernal Institute, University of Limerick (UL), Limerick V94 T9PX, Ireland
[c] Department of Chemical Sciences, School of Natural Sciences, University of Limerick (UL), Limerick, Ireland

ARTICLE INFO

Keywords:
Raman spectroscopy
Spectroelectrochemistry
EC-SOERS
Copper substrates

ABSTRACT

Raman enhancing strategies, such as Surface-Enhance Raman scattering (SERS), are a key piece for the development of spectroscopic and analytical strategies based on Raman spectroscopy, due to the intrinsic low sensitivity of the Raman scattering. Some years ago, our group reported an unexpected Raman enhancement process observed during the electrochemical oxidation of metallic electrodes, named Electrochemical Oxidation Surface-Enhanced Raman scattering (EC-SOERS). This Raman enhancement phenomenon was recently explained as an interaction of the analyte and the SERS dielectric substrate promoted by a metal cation. The elucidation of the origin of this enhancement is now leading to the development of new Raman enhancing substrates, such as copper-based substrates. In this work, we present an overview of the use of copper electrodes as EC-SOERS substrates. The presented strategies allow the electrosynthesis of SERS-active CuI nanocrystals on a metallic copper surface, which provides Raman enhancement for a wide number of molecules. The influence of the electrochemical conditions and the structure of the studied molecules are discussed. The use of CuSCN nanocrystals is also explored as substrates to promote Raman enhancement.

1. Introduction

Raman spectroscopy is an important spectroscopic technique developed in 1928 [1] and rarely used for the following 50 years. The low efficiency of Raman scattering required the use of long acquisition times and high analyte concentrations to obtain a suitable spectrum, which greatly limited the application of this technique. This problem was overcome in the mid-1970s, thanks to the development of lasers and to the discovery of the Surface-Enhanced Raman Scattering (SERS) phenomenon [2]. This phenomenon allows to increase the sensitivity of Raman spectroscopy by several orders of magnitude, which led to a huge development of Raman-based strategies for interfacial analysis. This has contributed to major advances in the development of sensors [3–9] and the study of surface phenomena [3,10–13].

Nearly half a century after the discovery of the SERS phenomenon, several phenomena have been identified that can enhance the Raman signal of molecules. Those effects have been classically grouped under two labels: electromagnetic enhancement (EM) and chemical enhancement (CM) [14–20]. Within EM are grouped changes in analyte polarizability due to the enhancement of the electric field generated by localized surface plasmon resonance (LSPR) and other plasmonic properties of SERS substrates. In CM, many electric field-independent Raman enhancement processes are group together, such as enhancement of static polarizability of the adsorbate compared to the free molecule or charge transfers (photoinduced or not) between the analyte and the substrate. Traditionally, it is assumed that EM is the most important of these two mechanisms, as it is able to generate enhancement factors greater than CM (10^9 versus 10^3) [15,21]. Works facing the quantification of the CM in SERS substrates normally found EF associated to this mechanism between 10 and 10^2, but some researchers have experimentally reached the theoretical maximum enhancement for CM, with experimental EF close to 10^3, which were attributed to resonant charge transfer processes [22].

The in-depth study of Raman enhancement phenomena has given rise to numerous instrumental techniques useful for the study of surfaces, such as Electrochemical-Surface Enhanced Raman Scattering (EC-

* Corresponding authors.
E-mail addresses: mpestebanez@ubu.es (M. Perez-Estebanez), acolina@ubu.es (A. Colina).
[1] Present address: Bernal Institute, University of Limerick (UL), Limerick, V94 T9PX, Ireland. Department of Chemical Sciences, School of Natural Sciences, University of Limerick (UL), Limerick, Ireland.

https://doi.org/10.1016/j.apsusc.2024.159442
Received 22 November 2023; Received in revised form 9 January 2024; Accepted 17 January 2024
Available online 20 January 2024

SERS) [3], Tip-Enhanced Raman Scattering (TERS) [23,24], Shell-Isolated Nanoparticle Enhanced Raman Scattering (SHINERS) [25,26] or other strategies that produces Raman enhancement of molecules by generating nanocrystals by oxidation of a metal surface, like Electrochemical-Surface Oxidation Enhanced Raman Scattering (EC-SOERS) [3,27,28]. This last phenomenon increases the Raman signal of molecules during the oxidation of a silver electrode in the presence of chloride or bromide anions [29]. The experimental conditions under which this type of enhancement takes place (anodic potentials, acidic pH) suggested that the origin of EC-SOERS is related to the semiconductor/dielectric structures electrogenerated during anodic treatment of the electrode, such as AgCl or AgBr nanocrystals. These silver halide crystals were proposed as SERS substrates in the early 80s [30] but the Raman enhancement was mainly related to the generation of Ag sols on the silver halide crystals. The use of dielectric and semiconductor materials as SERS substrates is a blooming field that has been strongly developed in the last two decades [19], and which is generating a great number of applications and new materials useful for SERS analysis [31–33]. In our latest work [27], EC-SOERS was explained as the amplification of the Raman signal mediated by metal cations adsorbed on semiconductor/dielectric structures generated during electrochemical oxidation of the electrode.

In literature, some Cu compounds (oxides and sulfides) have been proposed as SERS substrates [34,35]. However, to the best of our knowledge, Cu semiconductor/dielectric nanocrystals have been never proposed as SERS substrates following a strategy based on the electrochemical oxidation of the electrode surface. Until 2022, publications on EC-SOERS used exclusively silver electrodes as substrate [36–38]. In this work, we will demonstrate that EC-SOERS is not exclusive to this metal but can also be observed on copper electrodes. The influence of experimental conditions on this phenomenon will be studied and the use of different precipitating agents and the chemical selectivity of this metal for the generation of EC-SOERS of molecular species will be discussed, proposing very new methodologies for characterization, detection, and quantification of several molecules.

2. Materials and methods

2.1. Reagents and solutions

Perchloric acid ($HClO_4$, 60 %, Sigma-Aldrich), KI (>99 %, Labkem), KSCN (99 %, VWR), clopyralid (3,6 dichloropyridine-2-carboxilic acid, TCI, >98 %), benzoic acid (>99.5 %, Sigma-Aldrich), squaric acid (3,4-dihydroxi-3-cyclobutene-1,2-dione, 98+ %, Alfa Aesar), ciprofloxacin (98 %, Sigma-Aldrich), alizarin RS (>99.5 %, Acros Organics), carmine indigo (for analysis, Acros Organics), pyridine (99.8 %, Merck), methyl viologen hydrochloride (98 %, Sigma-Aldrich), nitrobenzene (>99 %, Acros Organics), isonicotinic acid (99 %, Alfa Aesar). All reagents were used as received, without further purification.

All solutions were prepared using ultrapure water obtained from a Millipore DirectQ purification system provided by Millipore (18.2 MΩ·cm resistivity at 25 °C).

2.2. Instrumentation

2.2.1. Time resolved Raman spectroelectrochemistry

In-situ time-resolved Raman spectroelectrochemistry (TR-Raman-SEC) was performed with a customized SPELEC-RAMAN instrument (Metrohm-DropSens), which included a 785 or a 638 nm laser source. The different lasers were used for experiments using different electrochemical substrates, searching a good compromise between signal/noise ratio and background fluorescence. For the measurements on silver electrodes, the 785 nm laser was used, and 638 nm for the copper electrodes. The laser power was set at 102 mW (325 W cm^{-2}) for the 785 nm laser and 20 mW (63.72 W cm^{-2}) for the 638 nm laser. Acquisition time was fixed at one second. This instrument was connected to a Raman probe (DRP-RAMANPROBE, Metrohm-DropSens). DropView SPELEC software (Metrohm-DropSens) was used to control the instrument, which allowed getting real-time and synchronized spectroelectrochemical data.

Two different electrochemical cells were used. For experiments using silver substrates, a home-made cell for silver screen-printed electrodes (AgSPE C013, Metrohm-DropSens) were used. These electrodes are made of a working electrode (WE) of silver ink (1.6 mm diameter), a glassy carbon counter electrode (CE) and a pseudo-reference of silver ink. The applied potential to these electrodes was corrected and referred to a reversible hydrogen electrode (RHE). For the experiments using copper substrates, a home-made Teflon cell with a capacity of about 3 mL were used. In this cell, a copper rod (99.999 %, metal basis, Alfa Aesar) of 3.2 mm diameter embedded in Teflon was used as WE. A gold strip (5 cm x 0.3 cm, 99.9 %, Goodfellow) was used as a CE and a home-made RHE was used as reference electrode. All potentials are referred to a RHE. All cyclic voltammetries were peformed at 0.02 Vs^{-1}.

Previous to each experiment, the copper rod WE was polished to mirror-like finish and then electropolished twice by applying +3 V vs Cu in a mixture of H_3PO_4 60 %, H_2SO_4 12 % and water 28 % for 10 s, using a copper foil as cathode.

2.2.2. Scanning electron microscopy

SEM images were acquired using a Field-Emission Scanning Electron Microscope (FESEM), model VP of ZEISS house. Images were taken with a secondary electron detector using a source power of 2.0 kV to avoid the excessive damage of the modified electrode surface.

3. Results and discussion

3.1. EC-SOERS on Cu/CuI substrates

During the last few years, several works about EC-SOERS on silver electrodes have been published [29,37,39]. In this work, we summarize the main features of the EC-SOERS on copper electrodes, expanding the knowledge of this phenomenon and studying the influence of the metallic substrate on it.

As a first example, clopyralid has been selected to illustrate the EC-SOERS phenomenon on copper electrodes. Clopyralid is a widely used herbicide that, to the best of our knowledge and despite its worldwide relevance, has not been previously reported using SERS or similar methodologies. So far, it has only been observed using EC-SOERS methodologies [27,39].

A typical EC-SOERS experiment on copper electrodes can be observed in Fig. 1. Fig. 1A shows the cyclic voltammetry (CV) of a copper electrode in 0.1 M $HClO_4$, + 5 mM KI and using 100 μM clopyralid as target molecule. While the electrochemical experiment was carried out, the Raman signal of the electrode surface was registered, performing a TR-Raman-SEC experiment.

The electrochemical behavior of the oxidation of copper in presence of iodide has been previously discussed [40–42]. Briefly, the formation of CuI crystals deposited on the electrode at around +0.10 V (vs RHE) can be observed, showing a maximum current around +0.15 V. Subsequently, the electrochemical oxidation of Cu to Cu^{2+}, starting at +0.40 V, is observed. In the cathodic sweep, several reduction processes are observed. The reduction of Cu^{2+} cations is observed at +0.35 V in the cathodic direction, but the precipitation of CuI (pKs = 12) causes the concentration of Cu^{2+} in solution to be very low, observing a very low cathodic peak around +0.20 V. Some weak cathodic peaks are found between +0.30 V and +0.00 V. These processes can be attributed to the reduction of CuI nanocrystals precipitated in solution during the oxidation of Cu [40–42]. Finally, at –0.20 V, the reduction of CuI formed on the electrode surface is observed.

In a classic SERS experiment involving oxidation–reduction cycles (ORC) on metallic electrodes, no Raman enhancement is usually expected at anodic potentials, because the generation of Cu nanoparticles

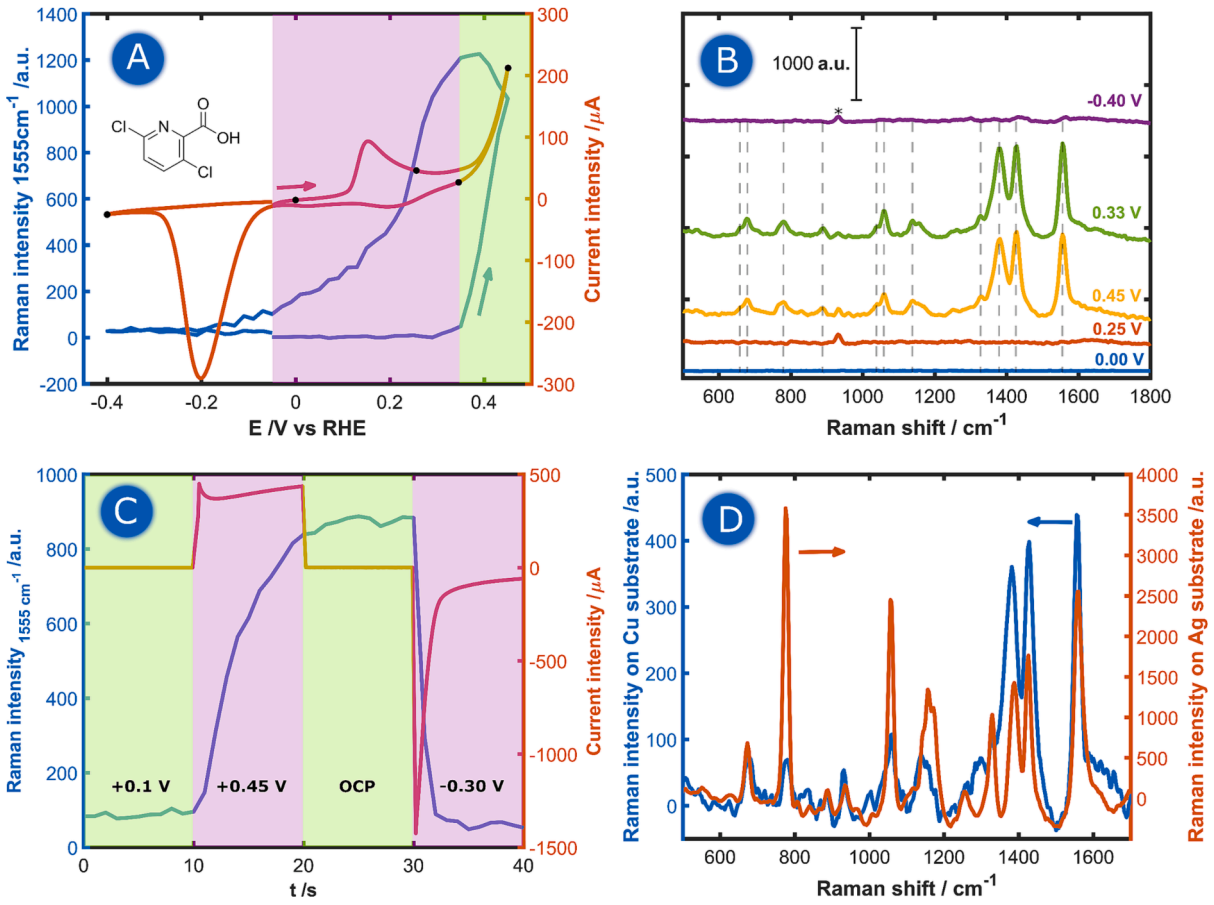

Fig. 1. (A) CV and voltaRamangram of clopyralid at 1555 cm^{-1} for a TR-Raman-SEC experiment on a Cu electrode. Inset: molecular structure of clopyralid. (B) Recorded Raman spectra at the potentials marked with black dots in the CV shown in A. Band marked with * corresponds to perchlorate anion. (C) Chronoamperogram and voltaRamangram at 1555 cm^{-1} for a multipulse chronoamperometry experiment. Electrolyte medium for (A), (B) y (C) were: 100 μM clopyralid + 5 mM KI + 0.1 M $HClO_4$. (D) Comparison between the EC-SOERS spectra of clopyralid observed on Cu (blue line) and Ag (orange line) electrodes. Electrolyte medium for Ag experiments was 90 μM clopyralid + 5 mM KBr + 0.1 M $HClO_4$, as reported in previous works [39]. All potentials are referred vs RHE.

(NPs) during the oxidation of the electrode is not expected. However, an unusual increase of the Raman signal is observed during the oxidation process. This behavior of the Raman signal is similar to the one observed during the oxidation of Ag in the presence of a suitable precipitating agent in acidic medium [28,39]. Fig. 1B shows the evolution of the Raman spectra on the electrode surface during the TR-Raman-SEC experiment. As can be seen, at the beginning of the experiment no Raman bands are detected, but when the potential is increased, the Raman spectrum of clopyralid is clearly enhanced (Fig. 1B). The evolution of the main Raman band of clopyralid (1555 cm^{-1}) during the CV is plotted in Fig. 1A (blue line). This representation is denominated as voltaRamangram, and evidence that the increment of the Raman signal coincides with the bulk oxidation of the electrode (green area, Fig. 1A). Later, during the cathodic scan, the Raman signal vanishes at potentials lower than –0.20 V (pink area, Fig. 1A).

This Raman enhancement observed during anodic oxidation of the electrode (EC-SOERS enhancement) has been explained in previous works [27]. So far, experiments have shown that the electrosynthesized CuI nanocrystals exhibit SERS properties, but the interaction between the CuI substrate and the target molecule is activated by the presence of Cu^{2+} ions, in a mechanism similar to the called “chloride activated SERS” [43], where chloride anions created active sites for the interaction between substrate and analyte. For this reason, the anodic oxidation of the Cu electrode is mandatory to observe the Raman enhancement. To study whether the decay of the Raman enhancement observed in Fig. 1A (pink area) is due to the application of lower potentials or simply due to time, we performed a multi-pulse chronoamperometry, shown in Fig. 1C. This figure clearly shows how the application of low potentials causes the decay of the Raman enhancement. This behavior is completely different to the one observed on Ag electrodes, where Raman signal decays at open circuit potential (OCP) [28,29]. In the case of EC-SOERS on Cu, the Raman signal does not decay at OCP, while Raman signal vanishes at OCP on Ag. We attribute this to the chemical properties of Cu^{2+} cation: Cu^{2+} ions do not form any precipitate with iodide in low concentrations, and therefore these ions remain in the solution while on silver, Ag^{+} ions precipitate in presence of the corresponding precipitating agent. This demonstrates that the presence of metal cations in the solution is a key parameter in EC-SOERS, since it promotes the adsorption of target molecules on the SERS active CuI nanocrystals. Only when Cu^{2+} ions are reduced, applying negative potentials (Fig. 1C) the Raman signal vanishes. This is the first difference in behavior respect to the EC-SOERS phenomenon on silver electrodes These results highlight the similarity between the EC-SOERS phenomenon on Cu and Ag electrodes (Raman enhancement at oxidation, dependence on the applied potential). However, there are more interesting differences between the two metals. For example, when the EC-SOERS spectrum of clopyralid is analyzed on the two metals, clear differences in the relative intensity of the Raman bands is observed (Fig. 1D), but not in the Raman shift of the bands. This indicates that the analyte does not undergo deep structural changes between the two systems, as this would change the number and position of its Raman bands, but it is undergoing a different Raman enhancement process, which selectively increases certain vibrational modes (e.g., different surface tilt or different influence of charge transfer processes).

To shed more light on the CuI crystals present on the electrode surface during the EC-SOERS enhancement, SEM images were made by stopping the potential at different points of the CV. These images are displayed in Fig. 2.

Fig. 2 shows that after the anodic peak at +0.15 V, a large number of pyramid or truncated pyramid-shaped CuI nanocrystals are formed, similar to the results reported in literature for other CuI anodic electrosynthesis techniques [40,41]. In this experiment, CuI nanocrystals have sizes ranging from 40 to 200 nm (Fig. 2B). During the electrochemical dissolution of the Cu surface, the shape and size of the CuI nanostructures evolve slightly, generating some plate-like structures at the oxidation vertex (Fig. 2C). Those plates disappear at lower potentials (Fig. 2E). The most noticeable change in the electrode surface is observed after the reduction of CuI at cathodic potentials. At this point, the well-defined CuI structures are no longer observable, and only chunks of reduced Cu are present in the electrode surface (Fig. 2D).

3.2. Influence of the electrochemical conditions on EC-SOERS

The generation of EC-SOERS substrates is highly dependent on the concentration of the precipitating agent used (KI, which allows the generation of CuI) to generate the nanocrystals [29,44]. To better characterize this influence on copper substrates, a study on the dependence of EC-SOERS intensity on KI concentration was performed. The influence of the KI concentration on the Raman response is summarized in Fig. 3. As an analyte for this study, we chose squaric acid (inset Fig. 3A), a small molecule whose derivatives exhibit various biological functions [45] and which exhibits high EC-SOERS activity. Experimental conditions are similar to that shown in Fig 1A but using varying concentrations of KI from 0 to 50 mM. As can be observed, in absence of iodide no EC-SOERS is detected, despite applying potentials high enough to massively oxidize the electrode (Fig. S1). This fact confirms that the formation of nanocrystals of CuI is a key factor for the enhancement of the Raman signal, similarly to the behavior observed for silver substrates, where the formation of AgCl or AgBr structures is mandatory to observe this Raman enhancement [28,44].

A small KI concentration of 10^{-4} M is enough to generate an appreciable Raman enhancement, which varies significantly as the amount of iodide increases. In the case of squaric acid, it is observed that the maximum EC-SOERS enhancement is achieved at 0.5 mM KI (yellow line, Fig. 3A), with the intensity of the Raman enhancement gradually decreasing with greater iodide concentrations. However, this study should not be considered as a general optimization of the conditions for observing EC-SOERS, as for each analyte the EC-SOERS behavior changes with KI concentration because of the chemical selectivity of the phenomenon.

To illustrate a completely different behavior with KI concentration, benzoic acid was chosen because in spite of being an EC-SOERS observable molecule, in this case, its EC-SOERS behavior is not affected by KI concentration in the range between 10 and 50 mM (Fig. 3B). This behavior is in good agreement to the one observed on silver electrodes, where for each molecule, the electrolytic conditions to show its maximum EC-SOERS enhancement are different [29]. From this result, it can be concluded that EC-SOERS response depends not only on

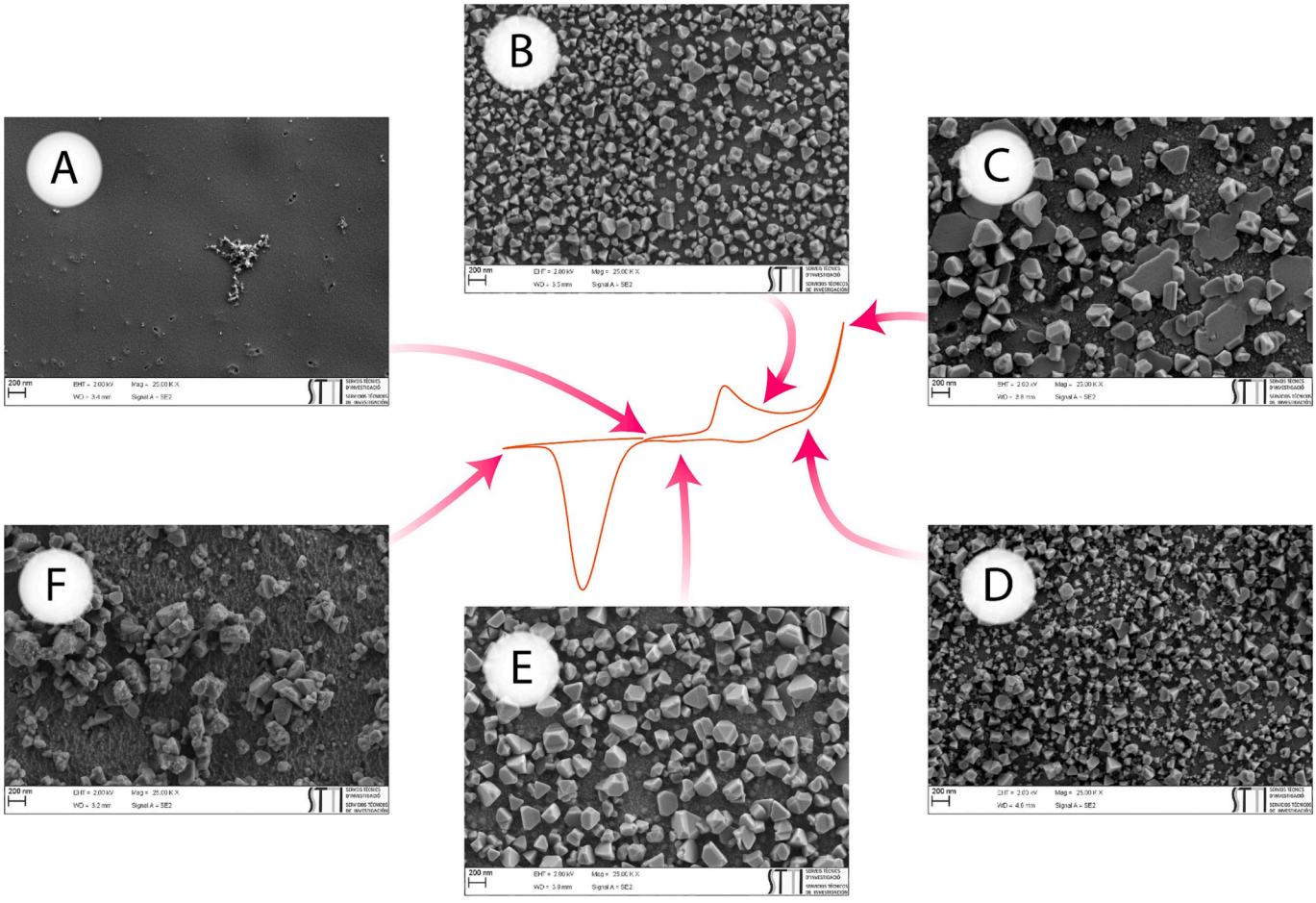

Fig. 2. SEM images of a Cu electrode at different potentials during a CV with 0.1 mM isonicotinic acid + 5 mM KI + 0.1 M $HClO_4$. (A) The electropolished electrode without further treatment. In the other figures the potential was stopped at (B) + 0.30 V, (C) + 0.45 V, (D) + 0.40 V (backward scan), (E) + 0.10 V (backwards scan), (F) −0.40 V. All scale bars represent 200 nm.

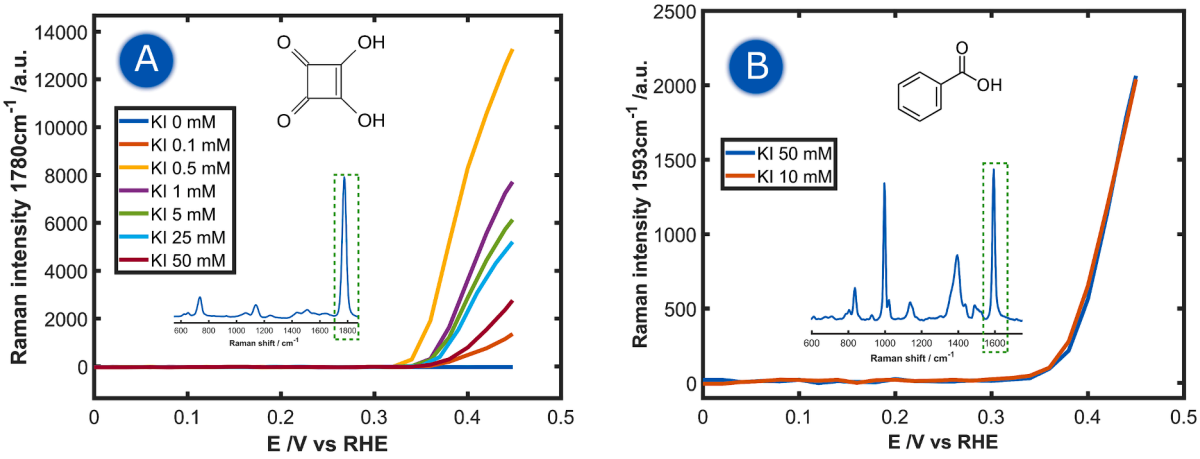

Fig. 3. Evolution of the Raman signal versus potential of 0.25 mM squaric acid (A) and 5 mM benzoic acid (B) under different KI concentrations. Inset spectra represent the most intense EC-SOERS spectra recorded for each analyte at + 0.45 V. Raman intensity of the bands marked in green box are plotted versus potential. Electrochemical conditions were x mM KI + 0.1 M $HClO_4$.

the KI concentration, but also on the chemical structure of the target analyte. Therefore, it is possible to generate an ad hoc EC-SOERS substrate for different analytes, trying to maximize the Raman enhancement of the analyte and decrease that of possible interferents by modulating the electrolytic conditions, giving rise to very interesting applications for analysis.

3.3. *Influence of the chemical structure of analyte*

EC-SOERS is a phenomenon that allows the Raman enhancement of a wide variety of molecules, being especially sensitive for the analysis of molecules with carbonyl and/or carboxyl groups. However, it was found that not all molecular structures are active in EC-SOERS. For example, molecules easy to observe in SERS experiments such as pyridine or

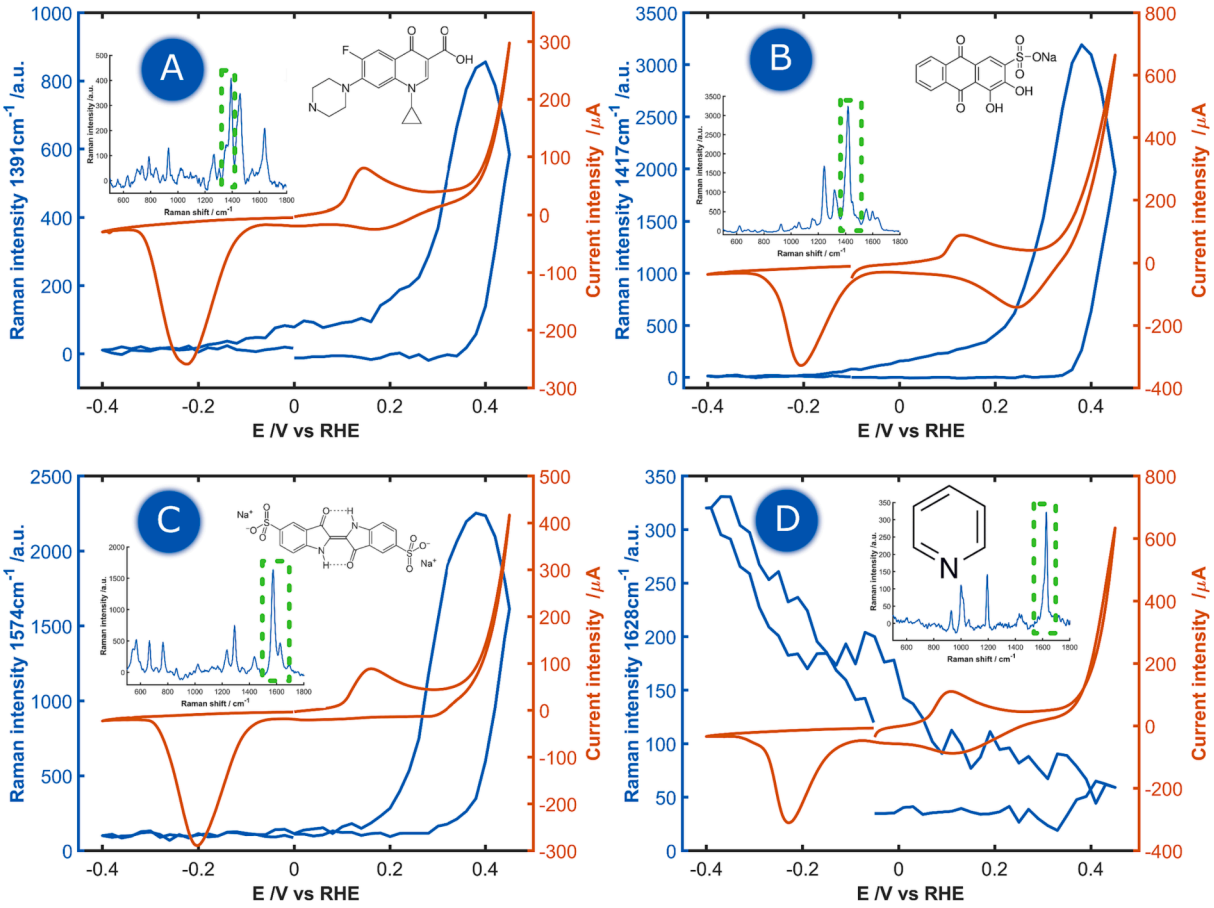

Fig. 4. Raman spectroelectrochemical response of different analytes on Cu substrates in 0.1 M $HClO_4$ + 5 mM KI. Orange lines represent CV responses, blue lines represent the Raman intensity of the analyte. Inset spectra represent the Raman spectra at the maximum enhancement potential. The Raman band plotted versus the potential is marked in green boxes for each analyte. Concentration of analytes: (A) 10 μM ciprofloxacin, (B) 10 μM alizarin RS, (C)10 μM indigo carmine, (D) 1 mM pyridine.

cyanide do not show Raman enhancement during the oxidation of Ag substrates [28].

An EC-SOERS behavior similar to that observed on Ag substrates is appreciated on Cu substrates. Fig. 4 shows the EC-SOERS responses for ciprofloxacin, alizarin RS, indigo carmine, and pyridine. We chose these analytes to provide a wide screening of functional groups (sulfone, carbonyl, carboxylate, heterocycles) and aromatic structures that can be detected using EC-SOERS. For the first three compounds, a clear increase of the Raman signal is observed during the oxidation of the electrode, even at low concentrations of analyte (~10^{-5} M).

In the case of pyridine, no Raman signal enhancement is observed at anodic potentials, even when using a high concentration of pyridine (10^{-3} M). Nevertheless, a clear increase in the Raman spectrum of pyridine is observed during the reduction of CuI structures, after the formation of potentially plasmonic Cu NPs [46,47], yielding a typical SERS response. Similar experiments show that other classical SERS probes, such as rhodamine 6G, also do not show EC-SOERS enhancement (Fig. S2).

The mechanism behind the EC-SOERS activity of different molecules has proven to be related to the interaction between target molecule and the CuI nanocrystals (or other metallic salt) [27]. This interaction is promoted by the adsorption of metal cations (Cu^{2+}) on the CuI crystal, giving the nanocrystal positive charge, and thus promoting the interaction with molecules with negative charge. This explanation is consistent with the non-EC-SOERS activity of pyridine (Fig. 4D), or rhodamine 6G (Fig. S2), which are neutral or positively charged molecules.

In general terms, all the analytes that have been studied with EC-SOERS on silver substrates also undergo Raman enhancement during the oxidation of copper substrates using KI as precipitating agent. Analytes with carboxyl, carbonyl or imine functional groups are generally easy to observe by EC-SOERS methodologies. Some examples of this behavior can be found in Fig. S3, including uric acid, related to gout disease, gallic acid, related to the organoleptic properties of wine, and bromophenol blue, an industrial dye, which provides an overview of the number of possible applications of this Raman enhancing methodology.

The development of copper EC-SOERS substrates has allowed us to discover that this metal particularly increases the sensitivity of the method for certain analytes. Fig. 5 shows some analytes that are a clear example of this behavior. Fig. 5A shows the EC-SOERS response of nitrobenzene on copper substrates. Similar to the previously presented analytes, this molecule shows a remarkable increase of the Raman signal at potentials above +0.35 V, where anodic oxidation of the copper surface takes place. However, these analytes do not show appreciable Raman enhancement when a similar experiment is performed on silver electrodes (Fig. 5B). We used several known precipitating agents for silver [27], but none of them was able to enhance the Raman signal of nitrobenzene over silver electrodes. We attribute this behavior to the preferent interaction of nitrobenzene with copper cations adsorbed over CuI crystals formed during the oxidation (Fig. 2), meanwhile no such interaction is observed for silver cations adsorbed over AgCl, AgSCN of $Ag_3Fe(CN)_6$ crystals [27]. These results reveal that the choice of metal substrate may be a key factor to modulate the chemical selectivity of the EC-SOERS phenomenon, allowing the selective detection of different functional groups. This chemical selectivity makes EC-SOERS a very promising technique to develop spectroscopic tools which can selectively study one target molecule.

3.4. Beyond CuI: KSCN as precipitating agent

The use of a precipitating agent that generates metal salt nanocrystals on the electrode surface is necessary to observe the EC-SOERS phenomenon. In the previous sections the relevance of CuI nanocrystals was discussed. However, this is not the only way to observe the EC-SOERS effect on Cu substrates. Experiments performed in the presence of KSCN have demonstrated its suitability as precipitating agent for the generation of EC-SOERS substrates. As an example, isonicotinic acid has been selected as target analyte to illustrate the performance of the substrate in this experiment. What is more, CuSCN substrates allows us to obtain a double fingerprint [38] of this analyte, as shown in Fig. 6.

Fig. 6A shows the CV and the evolution of two Raman bands, 1190 cm^{-1} and 1398 cm^{-1}, plotted versus potential. The CV shows the electrochemical dissolution of the electrode surface at potentials around +0.35 V, and the reduction of the generated cations centered at +0.10 V. Although a clear voltammetric peak corresponding to the electrogeneration of CuSCN is not observed because of the low SCN- concentration (1 mM), SEM images taken after the oxidation of the electrode reveal the generation of nanocrystalline structures of this material on the electrode surface (Fig. S4).

During the oxidation of the electrode, the increase in Raman intensity of several characteristic bands of isonicotinic acid are simultaneously observed (Fig. 6A, B) [48–50]. Later in the experiment, when the applied potential drops below +0.20 V, the reduction of the Cu^{2+} species and the CuSCN formed during the anodic sweep is observed (Fig. 6A, green line). At this point, the decrease of the EC-SOERS signal is observed (Fig. 6A, orange line), making the SOERS spectrum of the

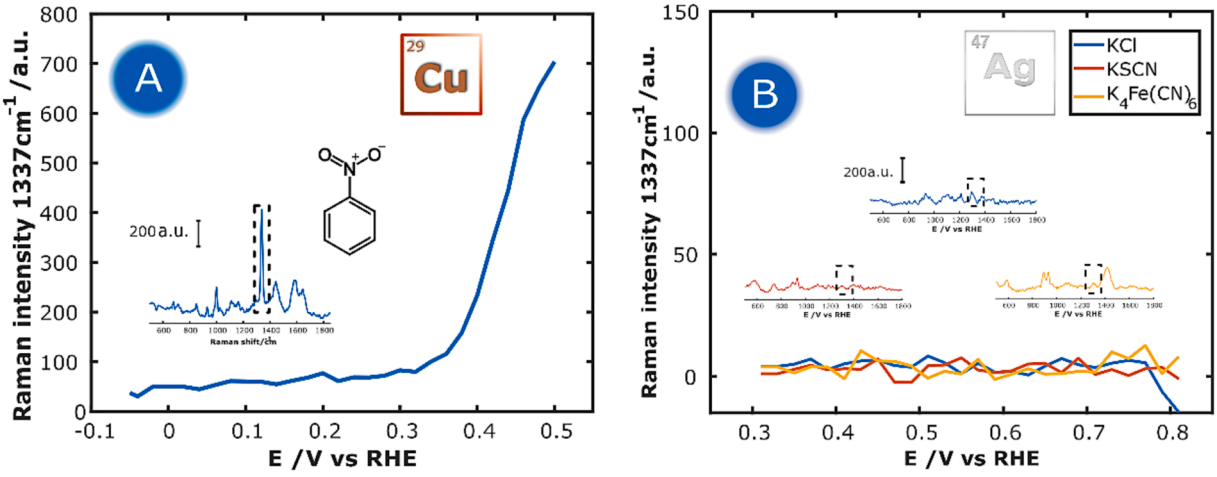

Fig. 5. Raman spectroelectrochemical response of 1 mM nitrobenzene over Cu electrodes in 0.1 M $HClO_4$ + 5 mM KI (A) and AgSPE (B) three different electrolytic media were explored over silver: 5 mM KCl, 0.5 mM KSCN and 0.5 mM $K_4Fe(CN)_6$. All solutions used 0.1 M $HClO_4$ as supporting electrolyte. Inset spectra represent the Raman spectra at the oxidation vertex, where maximum enhancement is observed. The Raman band plotted versus the potential are marked in dotted boxes for each analyte.

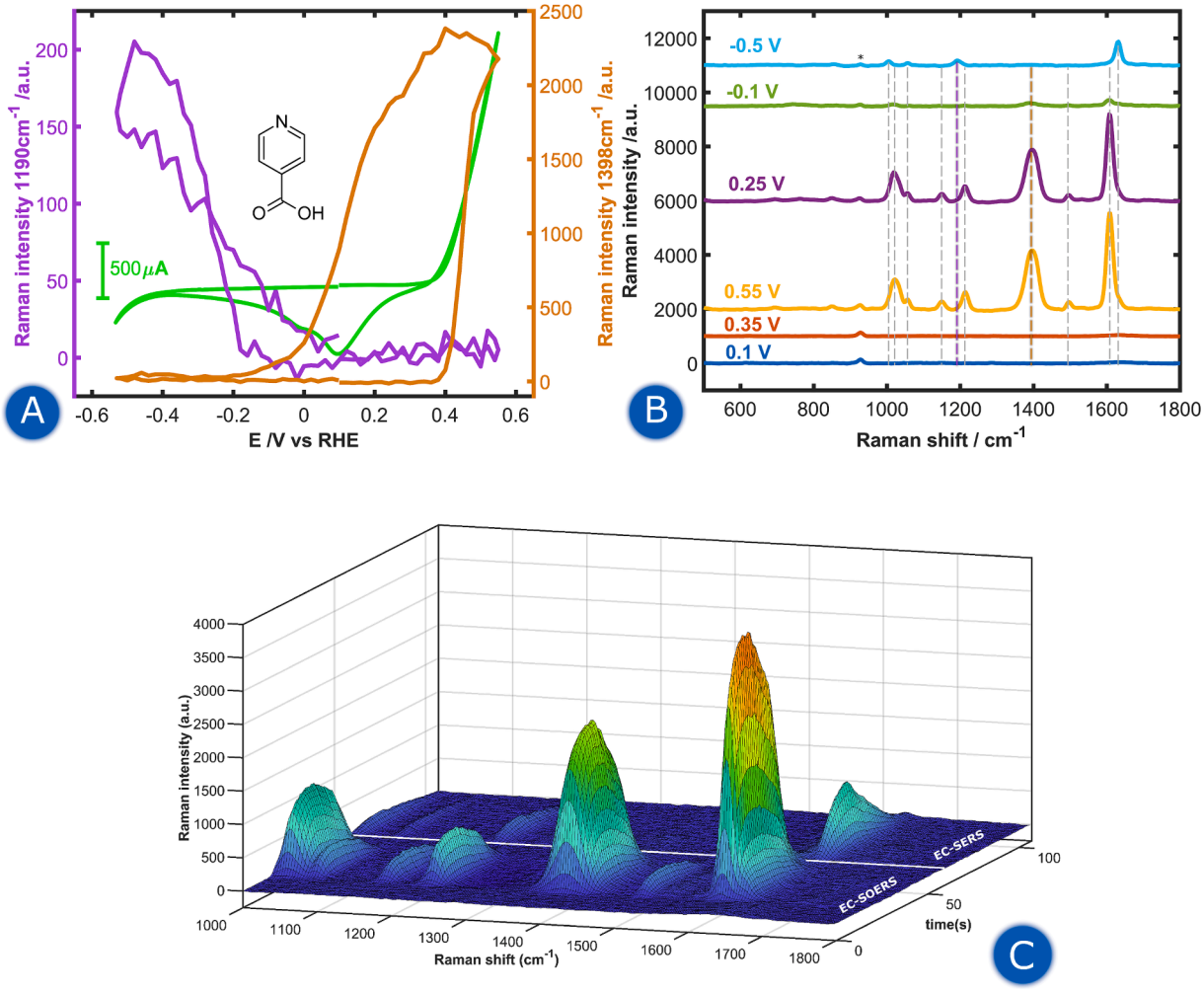

Fig. 6. EC-SOERS response of isonicotinic acid over Cu substrates in the presence of KSCN. (A) CV and evolution of two Raman bands vs the applied potential. (B) Raman spectra observed at the surface at different potentials. Raman bands marked in different color correspond to the represented signals in A. Raman band marked with * corresponds to perchlorate anion. (C) Surface plot of the full Raman spectra with the time. Electrochemical conditions: 0.1 mM isonicotinic acid + 0.1 M $HClO_4$ 0.1 M + 1 mM KSCN.

isonicotinic almost completely disappear (Fig. 6B, green line). This increase and subsequent decrease of the Raman signal in the anodic region is observed in Fig. 6A (orange line) for band at 1398 cm^{-1}. When the potential reaches a potential close to −0.20 V, a second Raman enhancement phenomenon is observed, corresponding to the EC-SERS effect of Cu(0) nanostructures generated during reduction [51]. Nevertheless, the observed spectra present some differences from those observed in the cathodic region (Fig. 6B). This is clearly observable for the band at 1190 cm^{-1}, which is only observable at negative potentials (Fig. 6A, purple line; Fig. 6B, cyan line, –0.50 V) This is a classic example of electrosynthesis of SERS substrates by applying an oxidation reduction cycle (ORC) [51]. This EC-SERS enhancement disappears when potentials above −0.20 V are reached, presumably due to the desorption of the analyte from the plasmonic substrate. The evolution of the Raman signals throughout this experiment can be seen more clearly in Fig. 6C, which shows the evolution of the full Raman spectrum during the whole experiment.

Previous studies have already shown that it is possible to obtain an EC-SOERS and EC-SERS response for a single analyte in the same experiment [38]. In the case of 5–fluorouracil, using Ag electrodes as substrate, significant differences between the two Raman spectra (EC-SERS and EC-SOERS) were observed. This strategy can also be carried out on Cu substrates, Fig. 6. In this case, using isonicotinic acid as target molecule, the spectral differences shown between the EC-SERS spectra observed at cathodic potentials (Fig. 6B, cyan line, –0.50 V) and EC-SOERS, observed at anodic potentials, (Fig. 6B, yellow and purple lines) can be attributed to a different protonation state. A more detailed comparison of the registered Raman spectra of isonicotinic acid in this experiment is presented in Table S1.

The band at 1398 cm^{-1}, corresponding to the C═O stretching of the carboxylate anion, reveals information about the protonation state of the carboxylate group, being visible only when the acid is in the deprotonated state [48,49]. Since this band is clearly visible in the Raman spectrum observed at anodic potentials (Fig. 6B, yellow and purple lines), we can conclude that the isonicotinic acid is deprotonated at these potentials due to the interaction with Cu^{2+} on the nanocrystal surface. Conversely, the absence of this band at potentials below 0.00 V shows that the carboxylate group is protonated in this region. We can perform a similar analysis of the protonation state of pyridine nitrogen by studying the shifting of band 8a of the aromatic ring (around 1615 cm^{-1}). It is well known that in pyridinic acids, this band is red-shifted when the pyridinic nitrogen is protonated [52]. In our experiment, this band is centered at 1610 cm^{-1} in the EC-SOERS spectra (positive potentials), while the band observed in EC-SERS (negative potentials) peaks at 1629 cm^{-1}, which evidences that the species observed in EC-SOERS is also deprotonated at the pyridine group, while the species observed in EC-SERS is N-protonated.

This experiment reveals that the use of KSCN allows us to clearly

observe the EC-SOERS phenomenon, being possible for some analytes to obtain a double fingerprint of the molecule in a single experiment, taking advantage of the capability of electrochemistry to generate two different Raman enhancement phenomena in the same experiment: EC-SOERS, during the oxidation of the electrode, and EC-SERS after the formation of plasmonic nanostructures of this metal. The results observed using KSCN as precipitating agent are also similar to those observed using KI. The experiment shown in Fig. 6 was carried out in a medium containing KI, obtaining analogous conclusions (Fig. S5), but observing a lower analytical enhancement factor ($4.8{\cdot}10^5$ in KSCN vs. 10^5 for EC-SOERS in KI, 1610 cm^{-1}).

4. Conclusions

In this work, multiple aspects about the use of copper-based EC-SOERS substrates have been discussed. The behavior of EC-SOERS enhancement on copper has been described in detail, providing an important number of analytes that can be analyzed by this methodology. The differences of copper-based EC-SOERS substrates with respect to silver-based substrates, more common in literature, have been pointed out. It has been concluded that both metals can selectively enhance certain Raman bands of the analytes, obtaining similar enhanced Raman spectra. Although the Raman shifts observed for the same analyte coincide for both metals. The influence of electrolytic conditions on Raman enhancement has also been discussed, concluding that this optimization must be done individually for each analyte.

The influence of the chemical structure of the analyte has also been studied, concluding that copper-based substrates allow observing the EC-SOERS response of analytes that do not undergo this Raman enhancement on silver substrates, such as, for example, nitrobenzene.

Finally, two new precipitating agents have been shown that allow the generation of copper-based EC-SOERS substrates: KI and KSCN, which allow obtaining a spectroscopic double fingerprint of certain analytes.

This study points to the existence of new substrates capable of increasing the Raman signal of specific analytes, which could be relevant in fields such as electrocatalysis, surface analysis or the development of new sensor devices for analytical purposes.

CRediT authorship contribution statement

Martin Perez-Estebanez: Writing – review & editing, Writing – original draft, Visualization, Validation, Methodology, Investigation, Formal analysis, Data curation, Conceptualization. **William Cheuque-pan:** Writing – review & editing, Supervision, Investigation, Formal analysis, Conceptualization. **Aranzazu Heras:** Writing – review & editing, Resources, Project administration, Funding acquisition, Formal analysis. **Alvaro Colina:** Writing – review & editing, Writing – original draft, Validation, Supervision, Project administration, Methodology, Investigation, Funding acquisition, Formal analysis, Data curation, Conceptualization.

Declaration of competing interest

The authors declare that they have no known competing financial interests or personal relationships that could have appeared to influence the work reported in this paper.

Data availability

Data will be available at the Universidad de Burgos data repository

Acknowledgements

Ministerio de Ciencia e Innovación and Agencia Estatal de Investigación (MCIN/AEI/10.13039/501100011033, PID2020-113154RB-C21), Junta de Castilla y León and European Regional Development Fund (Grant number: BU036P23), Ministerio de Ciencia, Innovación y Universidades (RED2022-134120-T) are gratefully acknowledged for funding this work. M. P.-E. acknowledges Junta de Castilla y León and European Social Found for his predoctoral contract. W. Ch. acknowledges Junta de Castilla y León for his postdoctoral fellowship (Grant BU297P18) and funding received from Marie Sklodowska-Curie postdoctoral fellowship (Grant MSCA-IF-EF-ST 2020/101031622).

Appendix A. Supplementary data

Supplementary data to this article can be found online at https://doi.org/10.1016/j.apsusc.2024.159442.

References

[1] C.V. Raman, K.S. Krishnan, A new type of secondary radiation, Nature 121 (1928) 501–502, https://doi.org/10.1038/121501c0.
[2] M. Fleischmann, P.J. Hendra, A.J. McQuillan, Raman spectra of pyridine adsorbed at a silver electrode, Chem. Phys. Lett. 26 (1974) 163–166, https://doi.org/10.1016/0009-2614(74)85388-1.
[3] C.L. Brosseau, A. Colina, J.V. Perales-Rondon, A.J. Wilson, P.B. Joshi, B. Ren, X. Wang, Electrochemical surface-enhanced Raman spectroscopy, Nat. Rev. Methods Primers 3 (2023) 79, https://doi.org/10.1038/s43586-023-00263-6.
[4] R. Moldovan, E. Vereshchagina, K. Milenko, B.-C. Iacob, A.E. Bodoki, A. Falamas, N. Tosa, C.M. Muntean, C. Farcău, E. Bodoki, Review on combining surface-enhanced Raman spectroscopy and electrochemistry for analytical applications, Anal. Chim. Acta 1209 (2022) 339250, https://doi.org/10.1016/j.aca.2021.339250.
[5] A.V. Markin, A.I. Arzhanukhina, N.E. Markina, I.Y. Goryacheva, Analytical performance of electrochemical surface-enhanced Raman spectroscopy: A critical review, TrAC - Trends Anal. Chem. 157 (2022) 116776, https://doi.org/10.1016/j.trac.2022.116776.
[6] M. Fan, G.F.S. Andrade, A.G. Brolo, A review on recent advances in the applications of surface-enhanced Raman scattering in analytical chemistry, Anal. Chim. Acta 1097 (2020) 1–29, https://doi.org/10.1016/j.aca.2019.11.049.
[7] W.A. Hassanain, C.L. Johnson, K. Faulds, D. Graham, N. Keegan, Recent advances in antibiotic resistance diagnosis using SERS: focus on the " Big 5 " challenges, Analyst 147 (2022) 4674–4700, https://doi.org/10.1039/D2AN00703G.
[8] M. Tavakkoli Yaraki, A. Tukova, Y. Wang, Emerging SERS biosensors for the analysis of cells and extracellular vesicles, Nanoscale (2022) 15242–15268, https://doi.org/10.1039/d2nr03005e.
[9] J. Perumal, Y. Wang, A.B.E. Attia, U.S. Dinish, M. Olivo, Towards a point-of-care SERS sensor for biomedical and agri-food analysis applications: a review of recent advancements, Nanoscale 13 (2021) 553–580, https://doi.org/10.1039/d0nr06832b.
[10] X.-J. Chen, G. Cabello, D.-Y. Wu, Z.-Q. Tian, Surface-enhanced Raman spectroscopy toward application in plasmonic photocatalysis on metal nanostructures, J. Photochem. Photobiol. C: Photochem. Rev. 21 (2014) 54–80, https://doi.org/10.1016/j.jphotochemrev.2014.10.003.
[11] D.P. Butcher, A.A. Gewirth, Nitrate reduction pathways on Cu single crystal surfaces: Effect of oxide and Cl−, Nano Energy 29 (2016) 457–465, https://doi.org/10.1016/j.nanoen.2016.06.024.
[12] C. Zhan, F. Dattila, C. Rettenmaier, A. Bergmann, S. Kühl, R. García-Muelas, N. López, B.R. Cuenya, Revealing the CO coverage-driven C-C coupling mechanism for electrochemical CO2 reduction on Cu2O nanocubes via operando raman spectroscopy, ACS Catal. 11 (2021) 7694–7701, https://doi.org/10.1021/acscatal.1c01478.
[13] J. Langer, D. Jimenez de Aberasturi, J. Aizpurua, R.A. Alvarez-Puebla, B. Auguié, J. J. Baumberg, G.C. Bazan, S.E.J. Bell, A. Boisen, A.G. Brolo, J. Choo, D. Cialla-May, V. Deckert, L. Fabris, K. Faulds, F.J. García de Abajo, R. Goodacre, D. Graham, A. J. Haes, C.L. Haynes, C. Huck, T. Itoh, M. Käll, J. Kneipp, N.A. Kotov, H. Kuang, E. C. Le Ru, H.K. Lee, J.-F. Li, X.Y. Ling, S.A. Maier, T. Mayerhöfer, M. Moskovits, K. Murakoshi, J.-M. Nam, S. Nie, Y. Ozaki, I. Pastoriza-Santos, J. Perez-Juste, J. Popp, A. Pucci, S. Reich, B. Ren, G.C. Schatz, T. Shegai, S. Schlücker, L.-L. Tay, K. G. Thomas, Z.-Q. Tian, R.P. Van Duyne, T. Vo-Dinh, Y. Wang, K.A. Willets, C. Xu, H. Xu, Y. Xu, Y.S. Yamamoto, B. Zhao, L.M. Liz-Marzán, Present and future of surface-enhanced Raman scattering, ACS Nano 14 (2020) 28–117, https://doi.org/10.1021/acsnano.9b04224.
[14] G. Demirel, H. Usta, M. Yilmaz, M. Celik, H.A. Alidagi, F. Buyukserin, Surface-enhanced Raman spectroscopy (SERS): an adventure from plasmonic metals to organic semiconductors as SERS platforms, J. Mater. Chem. C Mater 6 (2018) 5314–5335, https://doi.org/10.1039/c8tc01168k.
[15] S. Schlücker, Surface-enhanced Raman spectroscopy: Concepts and chemical applications, Angewandte Chemie – Int. Ed. 53 (2014) 4756–4795, https://doi.org/10.1002/anie.201205748.
[16] D.-Y. Wu, J.-F. Li, B. Ren, Z.-Q. Tian, Electrochemical surface-enhanced Raman spectroscopy of nanostructures, Chem. Soc. Rev. 37 (2008) 1025, https://doi.org/10.1039/b707872m.
[17] S.-Y. Ding, E.-M. You, Z.-Q. Tian, M. Moskovits, Electromagnetic theories of surface-enhanced Raman spectroscopy, Chem. Soc. Rev. 46 (2017) 4042–4076, https://doi.org/10.1039/C7CS00238F.

[18] D.-Y. Wu, X.-M. Liu, S. Duan, X. Xu, B. Ren, S.-H. Lin, Z.-Q. Tian, Chemical enhancement effects in SERS spectra: a quantum chemical study of pyridine interacting with copper, silver, gold and platinum metals, J. Phys. Chem. C 112 (2008) 4195–4204, https://doi.org/10.1021/jp0760962.
[19] X.X. Han, W. Ji, B. Zhao, Y. Ozaki, Semiconductor-enhanced Raman scattering: active nanomaterials and applications, Nanoscale 9 (2017) 4847–4861, https://doi.org/10.1039/C6NR08693D.
[20] I. Alessandri, J.R. Lombardi, Enhanced Raman scattering with dielectrics, Chem. Rev. 116 (2016) 14921–14981, https://doi.org/10.1021/acs.chemrev.6b00365.
[21] B. Sharma, R.R. Frontiera, A. Henry, E. Ringe, R.P. Van Duyne, SERS: materials, applications, and the future, Mater. Today 15 (2012) 16–25, https://doi.org/10.1016/S1369-7021(12)70017-2.
[22] M. Yilmaz, E. Babur, M. Ozdemir, R.L. Gieseking, Y. Dede, U. Tamer, G.C. Schatz, A. Facchetti, H. Usta, G. Demirel, Nanostructured organic semiconductor films for molecular detection with surface-enhanced Raman spectroscopy, Nat. Mater. 16 (2017) 918–924, https://doi.org/10.1038/nmat4957.
[23] P. Pienpinijtham, Y. Kitahama, Y. Ozaki, Progress of tip-enhanced Raman scattering for the last two decades and its challenges in very recent years, Nanoscale 14 (2022) 5265–5288, https://doi.org/10.1039/D2NR00274D.
[24] E. Bailo, V. Deckert, Tip-enhanced Raman scattering, Chem. Soc. Rev. 37 (2008) 921, https://doi.org/10.1039/b705967c.
[25] H. Zhang, S. Duan, P.M. Radjenovic, Z.Q. Tian, J.F. Li, Core-shell nanostructure-enhanced Raman spectroscopy for surface catalysis, Acc. Chem. Res. 53 (2020) 729–739, https://doi.org/10.1021/acs.accounts.9b00545.
[26] J.F. Li, Y.F. Huang, Y. Ding, Z.L. Yang, S.B. Li, X.S. Zhou, F.R. Fan, W. Zhang, Z. Y. Zhou, D.Y. Wu, B. Ren, Z.L. Wang, Z.Q. Tian, Shell-isolated nanoparticle-enhanced Raman spectroscopy, Nature 464 (2010) 392–395, https://doi.org/10.1038/nature08907.
[27] S. Hernandez, M. Perez-Estebanez, W. Cheuquepan, J.V. Perales-Rondon, A. Heras, A. Colina, Raman, UV–Vis absorption, and fluorescence spectroelectrochemistry for studying the enhancement of the raman scattering using nanocrystals activated by metal cations, Anal. Chem. (2023), https://doi.org/10.1021/acs.analchem.3c01172.
[28] J.V. Perales-Rondon, S. Hernandez, D. Martin-Yerga, P. Fanjul-Bolado, A. Heras, A. Colina, Electrochemical surface oxidation enhanced Raman scattering, Electrochim. Acta 282 (2018) 377–383, https://doi.org/10.1016/j.electacta.2018.06.079.
[29] M. Perez-Estebanez, S. Hernandez, J.V. Perales-Rondon, E. Gomez, A. Heras, A. Colina, Chemical selectivity in electrochemical surface oxidation enhanced Raman scattering, Electrochim. Acta 353 (2020) 136560, https://doi.org/10.1016/j.electacta.2020.136560.
[30] L. Dawn, W. Jian, X. Houwen, S. Xu, L. Fan-Chen, Enhancement origin of SERS from pyridine adsorbed on AgCl colloids, 1987.
[31] M. Shao, C. Ji, J. Tan, B. Du, X. Zhao, J. Yu, B. Man, K. Xu, C. Zhang, Z. Li, Ferroelectrically modulate the Fermi level of graphene oxide to enhance SERS response, Opto-Electronic Advances 6 (2023) 230094–230094. 10.29026/oea.2023.230094.
[32] S. Cong, Z. Wang, W. Gong, Z. Chen, W. Lu, J.R. Lombardi, Z. Zhao, Electrochromic semiconductors as colorimetric SERS substrates with high reproducibility and renewability, Nat. Commun. 10 (2019), https://doi.org/10.1038/s41467-019-08656-6.
[33] A. Bhakat, A. Chattopadhyay, Molecular cooperativity in the intense Raman scattering on the surface of an organic molecular microcrystal, Adv. Opt. Mater. (2023), https://doi.org/10.1002/adom.202301776.
[34] M. Chen, K. Li, Y. Luo, J. Shi, C. Weng, L. Gao, G. Duan, Improved SERS activity of non-stoichiometric copper sulfide nanostructures related to charge-transfer resonance, PCCP 22 (2020) 5145–5153, https://doi.org/10.1039/c9cp05930j.
[35] Y. Luo, L. Niu, Y. Wang, P. Wen, Y. Gong, C. Li, S. Xu, Regulating the work function of Cu2O films via crystal facet engineering with enhanced charge transfer and SERS activity, Appl Surf Sci 607 (2023), https://doi.org/10.1016/j.apsusc.2022.155095.
[36] S. Hernandez, J.V. Perales-Rondon, A. Heras, A. Colina, Electrochemical SERS and SOERS in a single experiment: a new methodology for quantitative analysis, Electrochim. Acta 334 (2020) 135561, https://doi.org/10.1016/j.electacta.2019.135561.
[37] S. Hernandez, J.V. Perales-Rondon, A. Heras, A. Colina, Determination of uric acid in synthetic urine by using electrochemical surface oxidation enhanced Raman scattering, Anal. Chim. Acta 1085 (2019) 61–67, https://doi.org/10.1016/j.aca.2019.07.057.
[38] M. Perez-Estebanez, W. Cheuquepan, J.V. Cuevas-Vicario, S. Hernandez, A. Heras, A. Colina, Double fingerprint characterization of uracil and 5-fluorouracil, Electrochim. Acta 388 (2021) 138615, https://doi.org/10.1016/j.electacta.2021.138615.
[39] M. Perez-Estebanez, W. Cheuquepan, M. Huidobro, J. Vicente Cuevas, S. Hernandez, A. Heras, A. Colina, Raman Spectroelectrochemical determination of clopyralid in tap water, Microchem. J. 183 (2022) 108018, https://doi.org/10.1016/j.microc.2022.108018.
[40] R.S. Vishwanath, S. Kandaiah, Electrochemical preparation of crystalline γ-CuI thin films through potential-controlled anodization of copper and its photoelectrochemical investigations, J. Solid State Electrochem. 20 (2016) 2093–2102, https://doi.org/10.1007/s10008-016-3218-3.
[41] N.T.M. Hai, S. Huemann, R. Hunger, W. Jaegermann, K. Wandelt, P. Broekmann, Combined scanning tunneling microscopy and synchrotron X-ray photoemission spectroscopy results on the oxidative CuI film formation on Cu(111), J. Phys. Chem. C 111 (2007) 14768–14781, https://doi.org/10.1021/jp072826u.
[42] J. Inukai, Y. Osawa, K. Itaya, Adlayer structures of chlorine, bromine, and iodine on Cu(111) electrode in solution: in-situ STM and ex-situ LEED studies, J. Phys. Chem. B 102 (1998) 10034–10040, https://doi.org/10.1021/jp982952l.
[43] A. Otto, A. Bruckbauer, Y.X. Chen, On the chloride activation in SERS and single molecule SERS, J. Mol. Struct. 661–662 (2003) 501–514, https://doi.org/10.1016/j.molstruc.2003.07.026.
[44] J.V. Perales-Rondon, S. Hernandez, A. Heras, A. Colina, Effect of chloride and pH on the electrochemical surface oxidation enhanced Raman scattering, Appl. Surf. Sci. 473 (2019) 366–372, https://doi.org/10.1016/j.apsusc.2018.12.148.
[45] J. Chasák, V. Šlachtová, M. Urban, L. Brulíková, Squaric acid analogues in medicinal chemistry, Eur. J. Med. Chem. 209 (2021), https://doi.org/10.1016/j.ejmech.2020.112872.
[46] G.M. Brown, G.A. Hope, D.P. Schweinsberg, P.M. Fredericks, SERS study of the interaction of thiourea with a copper electrode in sulphuric acid solution, J. Electroanal. Chem. 380 (1995) 161–166, https://doi.org/10.1016/0022-0728(94)03576-O.
[47] Z.Q. Tian, B. Ren, D.Y. Wu, Surface-enhanced Raman scattering: from noble to transition metals and from rough surfaces to ordered nanostructures, J. Phys. Chem. B 106 (2002) 9463–9483, https://doi.org/10.1021/jp0257449.
[48] L.K. Noda, O. Sala, SERS effect of isonicotinic acid adsorbed on a copper electrode, J Mol. Struct. 162 (1987) 11–17, https://doi.org/10.1016/0022-2860(87)85018-4.
[49] R. Wen, Y. Fang, Adsorption of pyridine carboxylic acids on silver surface investigated by potential-dependent SERS, Vib. Spectrosc. 39 (2005) 106–113, https://doi.org/10.1016/j.vibspec.2005.01.001.
[50] D.H. Dressler, Y. Mastai, M. Rosenbluh, Y. Fleger, Surface-enhanced Raman spectroscopy as a probe for orientation of pyridine compounds on colloidal surfaces, J. Mol. Struct. 935 (2009) 92–96, https://doi.org/10.1016/j.molstruc.2009.06.042.
[51] Y.-C. Liu, C.-C. Yu, S.-F. Sheu, Low concentration rhodamine 6G observed by surface-enhanced Raman scattering on optimally electrochemically roughened silver substrates, J. Mater. Chem. 16 (2006) 3546, https://doi.org/10.1039/b609417a.
[52] J. Barthelmes, W. Plieth, Field dependence of the protonation equilibrium of 2-pyridinecarboxylic acid on copper in sulfuric acid, J. Chem. Soc. Faraday Trans. 93 (1997) 1321–1324, https://doi.org/10.1039/a606016a.